Review of Scientific Instruments

Measurements of Ion Velocity Distributions in a Large Scale Laser-Produced Plasma

R. S. Dorst,[1, a)] P. V. Heuer,[1] D. B. Schaeffer,[2] C. G. Constantin,[1] and C. Niemann[1, b)]
[1)]*Department of Physics and Astronomy, University of California - Los Angeles, Los Angeles, California 90095, USA*
[2)]*Department of Astrophysical Sciences, Princeton University, Princeton, New Jersey 08540, USA*

(Dated: 18 August 2020)

Laser-produced plasma velocity distributions are an important, but difficult quantity to measure. We present a non-invasive technique for measuring individual charge state velocity distributions of laser-produced plasmas using a high temporal and spectral resolution monochromator. The novel application of this technique is its ability to detect particles up to seven meters from their inception (significantly larger than most laboratory plasma astrophysics experiments, which take place at or below the millimeter scale). The design and assembly of this diagnostic is discussed in terms of maximizing the signal to noise ratio, maximizing the spatial and temporal resolution, and other potential use cases. The analysis and results of this diagnostic are demonstrated by directly measuring the time-of-flight velocity of all ion charge states in a laser produced carbon plasma.

I. INTRODUCTION

Creation of a hot expanding plasma by laser ablation of a solid target is ubiquitous in laboratory astrophysics. The interaction of a laser-produced plasma (LPP) expanding into an ambient magnetized plasma is important in cases as diverse as the study of diamagnetic cavity formation[1], anomalous magnetic diffusion[2], plasma instability growth[3], and collisionless shock formation[4]. These systems are often hotter ($T_e \gtrsim 10$ eV) and denser ($n_e \gtrsim 10^{13}$ cm^{-3}) than those probed by traditional diagnostics (e.g. magnetic flux probes, Langmuir Probes, etc.), which also inherently disrupt the plasma during measurement. LPP experiments must instead rely on non-invasive diagnostics when traditional diagnostics would overly disrupt the dynamics or when the plasma is too hot/dense to permit physical probes.

In this paper, the design and assembly of a time-resolved monochromator to diagnose ion velocity distributions is discussed. We present results of time-of-flight (ToF) ion measurements from expanding laser plasmas. One distinguishing factor from conventional techniques (i.e. Langmuir probes, Thomson scattering) is the ability to separately diagnose different charge states within a composite plasma. By looking at self-emission spectral wavelengths for each of the species in our composite plasma, the velocity distributions and relative abundances of each ion species can be identified. This information is vital in order to further understand the creation and dynamics of the laser-produced plasma.

II. EXPERIMENTAL SETUP

This diagnostic was developed for use as part of a series of experiments studying instabilities in ion beams streaming parallel to ambient magnetic fields[3,5]. The LPP is created by focusing a high energy laser (1053 nm, 200 J, 25 ns FWHM) onto a high-density polyethylene (C_2H_4) target (Fig. 1). The composition of the LPP is determined by the intensity of the ablation laser[6], which for this experiment went up to $I_o = 10^{13}$ W/cm^2. This laser is operated by the University of California, Los Angeles (UCLA) High Energy Density Plasma (HEDP) Phoenix Laser Laboratory[7]. Based on this intensity, the most dominant ion species, in both population and total kinetic energy density[6], is C^{4+}. The resulting plasma expands though the ambient helium plasma of the Large Plasma Device (LAPD) at UCLA[8].

The LAPD consists of two cathodes (BaO and LaB_6) on either end of a 20 m, long 1 m diameter vacuum chamber that is capable of creating a quiescent and highly reproducible, steady-state ($\sim$ 15 ms), magnetized plasma at repetition rates up to 1 Hz. The LAPD can create a plasma up to electron density $n_e \sim 10^{13}$ cm^{-3}, electron temperature $T_e \sim 5-10$ eV, and ion temperature $T_i \sim 1$ eV.

The initially dense LPP ($n_i \sim 1.5 \times 10^{17}$ cm^{-3}) rapidly expands causing the leading edge of the ablated ion plume to become quite tenuous[6] ($n_i \leq 5 \times 10^{11}$ cm^{-3}) by the time it reaches the first optical diagnostic window (viewing port) at z = 32.5 cm. Nevertheless, the monochromator diagnostic can detect particles greater than seven meters from the target where the longitudinal dispersion has caused the density to drop further[5]. Measurements can be made through viewing windows spaced every 32.5 cm along the LAPD.

The spontaneous emission lines of interest for this study (isolated from other lines by at least the instrument function $\Delta\lambda = 0.3$ nm, and not containing significant fine structure) exist in the UV range ($225-245$ nm). The C^{4+} ion species was chosen for study based on experimental reasons, and of the observable self-emission lines, the 227.091 nm line was determined to be the brightest over a wide range of temperatures and densities. All measurements for these experiments were made through quartz windows, which were transparent down to $\sim$ 150 nm.

[a)]Electronic mail: rdorst@physics.ucla.edu.
[b)]Electronic mail: cniemann@g.ucla.edu.

LAPD Model white.png

FIG. 1. Cross section of experimental setup in the LAPD. The diagnostic collects light from the center of the LPP plume ($d_o = 110.0$ cm), and couples light to the monochromator through a convex lens. The light is wavelength filtered and collected by a PMT. The setup is placed at a distance of 32.5 cm along the blow-off axis ($-\hat{z}$ direction, anti-parallel to B_0) which is one of the viewing port locations where data can be collected.

III. DESIGN AND ASSEMBLY

The primary objective of this diagnostic is to measure the velocity of multiple concurrent charge states of fast ions. In our experiments, the ions are super-Alfvénic with speed $v/v_A > 1$, where $v_A = B/(4\pi m_i n_i)^{1/2}$ is the Alfvén speed, B is the ambient magnetic field, m_i is the ion mass, and n_i is the number density of the ions. This requires the diagnostic to have a temporal resolution of much less than one inverse ion cyclotron frequency ($\omega_{c,i}^{-1} = m_i c/q_i B$), where c is the speed of light, and q_i is the ion charge, and spatial resolution less than one ion inertial length ($\delta_i = v_A \omega_{c,i}^{-1}$).

There are three critical components of the diagnostic: the collection optics, the monochromator as a light filter, and a light detector system. The collection lens combined with the monochromator sets the spatial resolution, whereas the light detector system determines the temporal response and the light detection characteristics.

A. Collection optics

Coupling of light emitted from the source to the detector is most easily understood by tracing rays from the detector aperture back through the monochromator and into the plasma. Light emitted by the ions is collected by a spherical plano-convex lens and imaged onto the monochromator entrance slit. All calculations are performed under the assumption of an ideal lens (i.e. minimum spherical aberrations) and an optically thin plasma (i.e. negligible photon-ion collisions).

In order to transmit the image plane unaffected (i.e. without loss of light or resolution) through the monochromator, the collection optics should be positioned to match the f-number (N_f) of the monochromator($N_{f,m}$). In other terms, $d_i = 2rN_{f,m}$ where d_i is the distance between the lens and entrance slit of the monochromator, and r is the radius of the lens as can be seen in Fig. 1. Using the thin lens equation, the resulting distance from the lens to the object plane is $d_o = (2frN_{f,m})/(2rN_{f,m} - f)$, where f is the focal length of the collection optic(s).

The object distance is often set by experimental constraints. For instance, the closest a lens can physically be positioned to the axis of the LAPD chamber, while still being located outside of the chamber, is 0.5 m.

In the common case where the source of emission is spatially extended, characterizing the spatial resolution of the measurement system is necessary. This is especially crucial where there is spatial structure of interest. Conventionally a ray tracing algorithm would be used to calculate the collection volume of such a setup[9]. However, these can be cumbersome and computationally intensive. An alternative method has been utilized that is within 4% agreement of ray tracing algorithms[10].

FIG. 2. Sample pattern of accepted rays from a source displaced transverse to the collection axis. The effective area used to calculate the coupling efficiency uses the image of the monochromator slit.

The desired quantity is the collection efficiency (ε) for an arbitrary point within the source for the optical system under consideration (Fig. 2):

$$\varepsilon(x) = \frac{A_l(x,y,z)}{4\pi(x-d_i)^2} \tag{1}$$

where $A_l(x,y,z)$ is the area defined by the accepted light rays from an arbitrary point in space for all values $x > d_i$ (the location of the lens) and $\varepsilon(d_o + d_i) \equiv \varepsilon_o = 1$ at best focus. The collection efficiency for points outside of best focus is determined by projecting an image of the monochromator entrance slit onto a plane transverse to the collection axis (Fig. 2). Utilizing this technique, the collection volume boundary is defined to be where $\varepsilon = 1/e \approx 0.37$

For the setup used in experiments conducted on the LAPD, the light was collected through a 200 mm focal length lens to a 1/4 m Acton spectrometer (1200 grooves/mm grating blazed at 500 nm). The entrance slit was set to be 10 μm with a height of 4 mm. The resulting collection volume was determined to be 0.23 cm^3 along the line of sight, with a maximum cross section of 2.8 cm $\times$ 2.2 μm (corresponding to the height and width of the slit, respectively).

B. Detector comparison

There are many important factors to weigh when deciding upon a light detector, including: temporal response, quantum efficiency, signal to noise, spectral range, and radiant flux being observed. The two metrics that most compactly encompass these quantities are the signal to noise ratio (S/N) and the equivalent noise input (ENI). The ENI (also known as noise equivalent power) is the minimum input light flux at which you receive a S/N of unity for a detector. In comparing two commonly used light detectors - the avalanche photodiode (APD) and the photomultiplier tube (PMT) - it was determined that the PMT outperformed the APD under our experimental conditions.

The signal output by an APD is $I_s = MR(\lambda)P_i$, where M is the gain, $R(\lambda)$ is the responsivity at a given wavelength (λ)

and P_i is the input power. Depending on the value of P_i, the detector noise will be dominated by either detector dark noise (I_d) at low levels, or photon shot noise at higher levels.

$$\frac{S}{N}_{APD} = \frac{MR(\lambda)P_i}{\sqrt{(2q\Delta B(I_d + R(\lambda)M^2P_iF))}} \quad (2)$$

The S/N is given by Eq. 2 where q is the elementary charge, ΔB is the bandwidth, and F is the excess noise factor, which describes the statistical noise due to multiplication process and is given by $F = Mk + (2-1/M)(1-k)$, where k is the ionization rate ratio[11]. The minimum detectable optical power, P_{min} can be calculated from setting Eqn. 2 equal to 1. This results in

$$P_{i,APD,min} = \frac{q\Delta BF}{R(\lambda)} + \frac{\sqrt{q^2\Delta B^2F^2 + 2q\Delta BI_dM^{-2}}}{R(\lambda)} \quad (3)$$

Since the dark current will dominate for low level light signals, this can be estimated as:

$$P_{i,APD,min} = \frac{\sqrt{2q\Delta BI_d}}{MR(\lambda)} \quad (4)$$

The S/N for the PMT case is given by Eqn. 5 where S_p is the anode radiant sensitivity, I_{da} is the anode dark current, and μ is the gain[12].

$$\frac{S}{N}_{PMT} = \frac{S_pP_i}{\sqrt{(2q\Delta B\mu F(S_pP_i + 2I_{da}))}} \quad (5)$$

Unlike the APD case where one term in the noise dominates over the other for low input power, both noise sources have to be taken into consideration when rearranging for P_i, min[12].

$$P_{i,PMT,min} = \frac{q\mu F\Delta B}{S_p} + \frac{\sqrt{(q\mu F\Delta B)^2 + 4qI_{da}\mu F\Delta B}}{S_p} \quad (6)$$

Where F and S_p are highly wavelength dependent. Once a specific wavelength of interest has been chosen, the values for the majority of terms in equations 2 and 5 are determined. However, the PMT is designed to be able to have certain characteristics, namely bandwidth, changed by an external circuit. The bandwidth of this type of ciruit is given[11] by $\Delta B = 0.35/\tau_{RC} = 0.35/R_{tot}C_{tot}$, where τ_{RC} is the characteristic time of an RC circuit, R_{tot} is the total resistance and C_{tot} is the total capacitance.

Both the APD and PMT have a low output capacitance ($\sim$ 0.1 – 100 pF and $\sim$ 1 – 20 pF, respectively). Therefore, the total capacitance is dominated by the connecting BNC cable (C_{BNC}), which typically has a capacitance/length value in the 100 – 300 pF/m range.

A PMT has a series of smaller resisters that add up to have high terminal impedance ($\sim$ 300 kΩ). By impedance matching this to an external circuit (oscilloscope, data-acquisition-system, etc.) the τ_{RC} can be manipulated by adding a parallel shunt resistor. For instance: assuming the use of an oscilloscope that has 1 MΩ impedance capabilities, different shunt resistors can be placed in parallel so as to set the total resistance of the system. This combined with the C_{BNC} will set the bandwidth, and therefore the S/N of the setup. Shunt resistors ranging from 500 Ω – 10 kΩ therefore result in an effective bandwidth of 23.33 MHz –1.2 MHz respectively.

	Hamamatsu S12053-10 (APD)	Hamamatsu R7518 (PMT)
$R(\lambda)$ *or* S_p (A/W)	0.14	$5.1x10^5$
Gain (M or μ)	50	$1.2x10^7$
I_D (nA)	1.0	0.2
F	3	1
A_d (mm^2)	0.79	192
S/N at 1 μW	3.8	237

TABLE I. Comparison of S/N of the Hamamatsu $S12035-10$ APD and $R7518$ PMT. The terminal resistor used to calculate is $1k\Omega$, giving a $\tau_{RC} = 36$ *ns*. All values taken at 227.1 *nm* wavelength value.

In contrast, the terminal circuitry in an APD is an active low-pass filter with amplification. The output impedance is low ($\sim$ 50 Ω) which does not offer the same adaptability to external circuitry as with high impedance. The output impedance dominates τ_{RC} and therefore the bandwidth is fixed.

This straight-forward adjustment to the bandwidth, and therefore the S/N, by changing out the shunt resistor is a desired quality of this diagnostic, which is satisfied by the PMT. This offers flexibility to configure the setup for varying levels of light detection. For laser experiments run on the LAPD, this flexibility allows for measuring a hot, dense plasma as well as a cold, tenuous plasma with minimal adjustments.

The final aspect to be weighed is the detector active area A_d. This is important to match to the image size at the detector in order to maximize the light that is being collected. Generally, $A_{d,PMT} > 100\ A_{d,APD}$. Due to a small active area, many APDs waste collected light and therefore have a much smaller effective P_i. This will need to be taken into account when comparing the S/N_{eff}.

Under expected values of light flux (1 μW) and detector properties for PMTs and APDs (Table 1) that fit in this setup, it was determined that $S/N_{PMT} >> S/N_{APD}$. In cases of high radiant flux leading to an anode output current of $I_{a,out} >$ 1 μA or for time resolution of $<$ 1 ns, an APD would be the desirable detector.

IV. CALCULATING VELOCITY FROM DETECTOR SIGNALS

This diagnostic was tested during experiments (Fig. 1) where a laser (10^{12} W/cm^2, 1053 nm) ablates a C_2H_4 (plastic) target. The resulting LPP streams transverse to the focal axis of the monochromator. The dominant charge state[6], both in terms of kinetic energy density and population fraction, is C^{4+}. As LPP particles pass through the collection volume, light of characteristic wavelengths is emitted through self-

FIG. 3. Top: Comparison of raw (blue) and corrected (orange) C^{4+} ($\lambda = 227.1$ nm) velocity distributions from self-emission signals. The correction shifts the velocities by up to 20%. Bottom: Relative difference between the two profiles above.

FIG. 4. a) Time traces of C^{+4} ($\lambda = 227.1$ nm) ion self-emission measured at three distances from the target. b) Corresponding (corrected) velocity traces for each of the time traces.

emission. The light is collected by the lens, filtered through the monochromator and coupled to the PMT.

Based on the geometry of the LAPD, diagnostic ports are only available at specific intervals along the z-axis, which determines the spatial frequency of measurements. Once a given distance has been selected, a time trace of the self-emission of a specified LPP ion species (Fig. 4a) is recorded. Temporal profiles of ion self-emission are recorded with a time resolution ranging from $10-200$ ns. The self-emission profiles can be transformed into velocity data by using the time-of-flight based on the distance. However, calculating the velocity bins in this way weighs slower particles more than faster particles, as they spend more time in the collection volume. This effect can be corrected by using a velocity-dependent time-integration method, wherein we multiply the amplitude by the velocity. The correction shifts the velocity distributions to larger values, which is shown in the bottom plot of Fig. 3.

Other diagnostics, such as Langmuir probes, are capable of producing ion velocity traces[5]. The differentiating factor for the diagnostic being presented is the ability to distinguish between ion species based on the emitted spectral line, the control over the S/N and bandwidth of each measurement, and the linearity in response (Langmuir probes have a nonlinear response at higher currents due to charge accumulation). In Fig. 4, three different time profiles and corresponding velocity profiles of C^{4+} at different distances from the target are displayed. These were taken at the same wavelength ($\lambda = 227.1$ nm), but with 3 different shunt resistors ($500\ \Omega$ for blue, 5 kΩ for orange, and 10 kΩ for green). Although the S/N and bandwidth of these measurements vary significantly, the velocity distributions are mostly unaffected. The furthest measurement of C^{4+} was at 715 cm from the target, limited by the viewing ports of the LAPD.

V. DISCUSSION AND CONCLUSION

The system of a monochromator using a photomultiplier tube as a detector was designed to measure time-of-flight (TOF) velocity of laser-produced plasma (LPP) ions streaming transversely to the collection plane, in a magnetized ambient plasma. The diagnostic well resolved the dynamics of the laser plasma ions spatially (~ 0.1 mm^3) and temporally ($\sim 10-200$ ns depending on the chosen detector bandwidth) and provided a S/N ratio greater than an avalanche photodiode detector (see Sec. III).

There is no direct way of measuring a localized temperature and density with this diagnostic. However, by comparing the measured spectrum to collisional-radiative modeling software, the temperature and density can be inferred[13]. Temporally and spatially resolved spectra can be collected by varying the monochromator wavelengths across many laser shots. In order to properly compare the measured spectra to a model, the responsivity (or the electrical output per optical input) must be determined. This is important in order to compare the correct absolute amplitudes of the spectral lines. This calibration can be accomplished using two well-characterized light sources: one being a continuous source to get the wavelength dependence, and the other being a narrow band light source to determine how the instrument function affects the power density[14]. Developing this technique will be a subject for future work.

VI. ACKNOWLEDGEMENTS

This work was supported by the Defense Threat Reduction Agency, Lawrence Livermore National Security LLC, and the United States Department of Energy (DOE) under Contract No. DE-SC0017900.

The Peening laser was made available by the Naval Information Warfare Center Pacific under Contract No. NCRADA-NIWCPacific-19–354.

VII. DATA AVAILABILITY STATEMENT

The data that support the findings of this study are available from the corresponding author upon reasonable request.

VIII. REFERENCES

[1] A. S. Bondarenko, D. Schaeffer, and E. E. et al., Nature Phys. **13**, 573 (2017).
[2] G. Dimonte and L. G. Wiley, Phys. Rev. Letters **67**, 13 (1991).
[3] P. V. Heuer, M. S. Weidl, R. S. Dorst, D. B. Schaeffer, S. Tripathi, S. Vincena, C. Constantin, C. Niemann, L. W. III, and D. Winske, The Astrophysical Journal Letters **891**, 1 (2020).
[4] C. Niemann, W. Gekelman, C. G. Constantin, E. T. Everson, D. B. Schaeffer, A. S. Bondarenko, S. E. Clark, D. Winske, S. Vincena, B. V. Compernolle, and P. Pribyl, Geophysical Research Letters **41**, 7413–7418 (2014).
[5] P. Heuer, M. Weidl, R. Dorst, D. Schaeffer, A. Bondarenko, S. Tripathi, B. V. Compernolle, S. Vincena, C. Constantin, C. Niemann, and D. Winske, Physics of Plasmas **25**, 032104 (2018).
[6] D. B. Schaeffer, A. S. Bondarenko, E. T. Everson, S. E. Clark, C. G. Constantin, and C. Niemann, J. Appl. Phys. **120**, 043301 (2016).
[7] C. Niemann, C. G. Constantin, D. B. Schaeffer, and et. al., Journal of Instrumentation **7**, P03010 (2012).

[8]W. Gekelman, P. Pribyl, Z. Lucky, M. Drandell, D. Leneman, J. Maggs, S. Vincena, B. V. Compernolle, S. K. P. Tripathi, G. Morales, T. A. Carter, Y. Wang, and T. DeHaas, Review of Scientific Instruments **87**, 025105 (2016).
[9]P. B. Farnsworth, B. W. Smith, and N. Omenetto, Spectrochimica Acta. **45B**, 1151 (1990).
[10]M. J. Colgan, Rev. Sci. Instrum. **63**, 5311 (1992).
[11]H. P. K.K., "Mppc)," Hamamatsu Photonics K.K. (1994).
[12]A. Ghassemi, K. Sato, and K. Kobayashi, "Photomultiplier technical handbook third edition (3a)," Hamamatsu Photonics K.K. (2016).
[13]E. M. Sciamma, R. D. Bengston, W. L. Rowan, A. Keesee, and C. A. L. et al., Rev. Sci. Instrum **79**, 10E324 (2008).
[14]M. Sassi and J. W. Daily, J. Quant. Spectrosc. Radiat. Transfer **40**, 426 (1998).

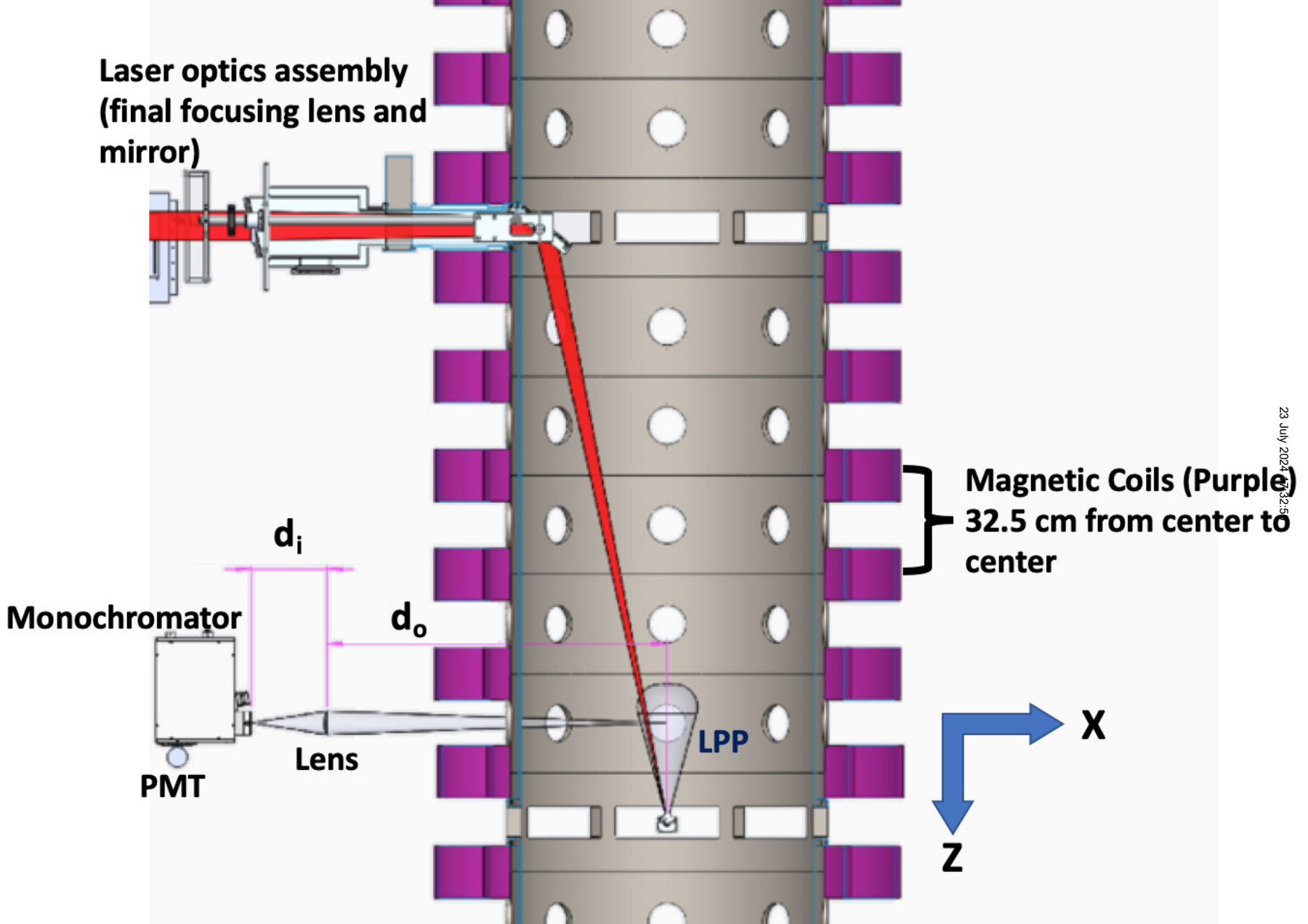
Laser optics assembly (final focusing lens and mirror)
Magnetic Coils (Purple) 32.5 cm from center to center
d_i
d_o
Monochromator
PMT
Lens
LPP
X
Z

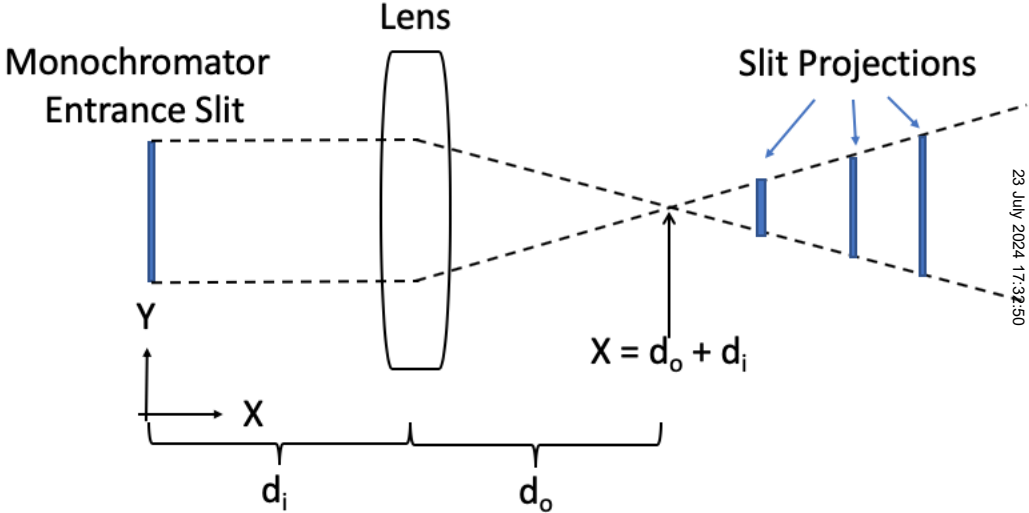

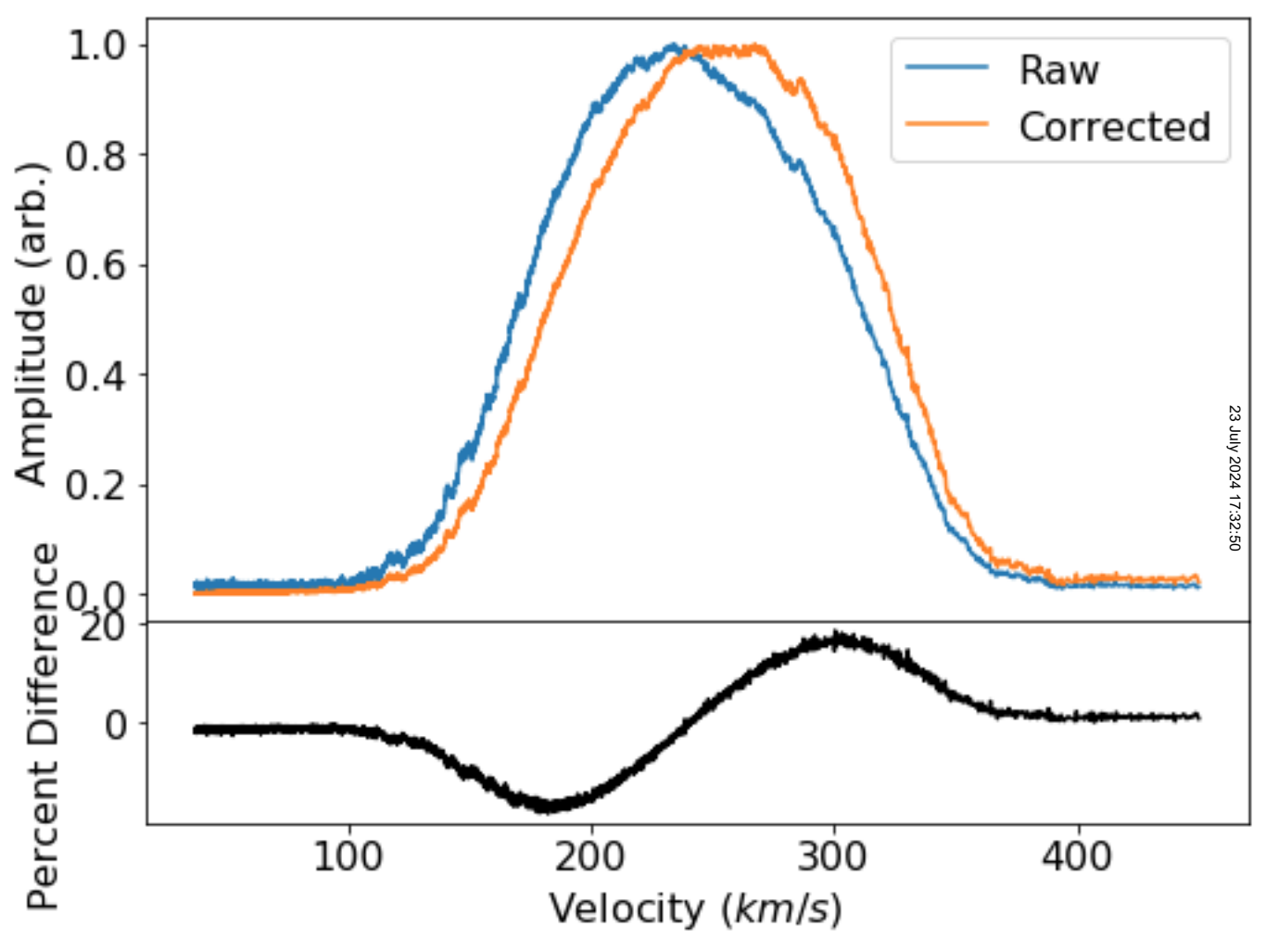
Raw
Corrected
Amplitude (arb.)
1.0
0.8
0.6
0.4
0.2
0.0
Percent Difference
20
0
100
200
300
400
Velocity (km/s)
23 July 2024 17:32:50